Periodic poling of magnesium-oxide-doped lithium niobate

Koichiro Nakamura,[a] Jonathan Kurz, Krishnan Parameswaran, and M. M. Fejer
Edward L. Ginzton Laboratory, Stanford University, Stanford, California 94305-4085

(Received 6 August 2001; accepted for publication 9 January 2002)

In this article, poling characteristics and periodic poling of magnesium-oxide-doped lithium niobate (MgLN) are described. Periodic poling was done by the electric field method, with which uniform gratings were produced. The domain wall velocity as a function of poling field was measured and used to determine conditions for self-terminating periodic poling. A computational model for the self-termination method is also discussed here. In the experiment, it was found that thermal history prior to poling has a significant influence on the poling quality. © *2002 American Institute of Physics.* [DOI: 10.1063/1.1456965]

I. INTRODUCTION

Periodically poled ferroelectric materials are of importance for nonlinear optical frequency conversion by quasiphase matching (QPM). This technique allows the use of the largest nonlinear optical coefficient of the material and noncritical phase matching of any interaction within its transparency range. Periodically poled lithium niobate (PPLN) has been commonly used for QPM devices because of its large nonlinear optical coefficient, $d_{33}=28$ pm/V, its high optical quality, and the availability of large crystals. Several impressive applications of PPLN have been reported. However, photorefraction and difficulty of fabrication of thick PPLN limit its use for high power, short wavelength, and room temperature operation, so it is of interest to explore alternative materials for QPM.

Magnesium-oxide-doped lithium niobate (MgLN) has attractive material properties for QPM devices, including a high resistance to photorefractive damage and a low coercive field. Bryan *et al.* reported a hundred-fold increase in photoconductivity of MgLN as compared to that of undoped congruent lithium niobate (LN).[1] Since the photorefractive index change is proportional to the ratio of the photogalvanic current to the photoconductivity,[2] MgLN has a higher photorefractive damage threshold. It also appears that MgLN has much lower green-induced infrared absorption (GRIIRA) than does LN. These features are important in blue/green light generation by second-harmonic generation as photorefractive damage and GRIIRA limit the available second-harmonic power. There have been several reports of blue light generation by periodically poled MgLN (PPMgLN), both in bulk[3–5] and waveguide[6–11] devices. The low coercive field makes it possible to fabricate thick PPMgLN crystals. Domain inversion with an electric field as low as 4.45 kV/mm was reported by Kurimura *et al.*[12] Periodic poling of 1-mm-thick MgLN was recently reported by Hirano *et al.*[13] They achieved high-average-power, room-temperature operation of a PPMgLN optical parametric oscillator, in which the material showed high resistance against the photorefractive effect.[14]

In this article, poling characteristics and periodic poling of MgLN are described. Uniform grating patterns were obtained using an electric-field poling method. In Sec. II, a relation between domain wall velocity and applied electric field (the velocity–field curve) is presented. In Sec. III, this curve is used to determine the conditions for self-termination of periodic poling. Periodic poling of MgLN is described in Sec. IV. In Sec. V, we discuss the factors which influence the poling quality.

II. POLING CHARACTERISTICS OF MgLN

The poling was done by the conventional electric-field method. The poling voltage was applied with a uniform electrode consisting of LiCl electrolyte. The crystal had 5 mol. % MgO doping (manufactured by Yamaju Ceramics) and the crystal thickness was 0.3 mm. The velocity–field curve provides useful insight into the dynamics of the poling process. The domain wall velocity was measured by the Miller and Savage method:[15] the sample is poled for a time T, the surface is etched, the progress of the domain wall L is measured, and the velocity is taken as L/T. The Miller and Savage method sometimes underestimates the domain wall velocity.[15] This behavior is likely related to the ''flip back'' phenomenon, where some or all of a reversed domain can revert to its original orientation when the poling field is abruptly dropped to zero.[16] Care was taken to maintain a field after the poling pulse that was large enough to prevent flip back but low enough that further growth of the domain was negligible. Another complexity, which arises with MgLN but not with LN, is that there is a delay between the first application of poling voltage and the observation of significant growth of the poling current. It appears that this delay reflects a time dependence of the initial nucleation of new domains in MgLN, on a time scale that is slow compared to that in LN. In domain inversion of LN, the domain nucleation is time and field independent for fields from 24 to 64 kV/mm.[17] In our experiment, a second-long poling field of 6.7 kV/mm was applied prior to the domain wall velocity measurement to avoid the slow starting region of the poling.

[a]Present address: Lightbit Corporation, Mountain View, CA., 94043; electronic mail: koichiro@lightbit.com

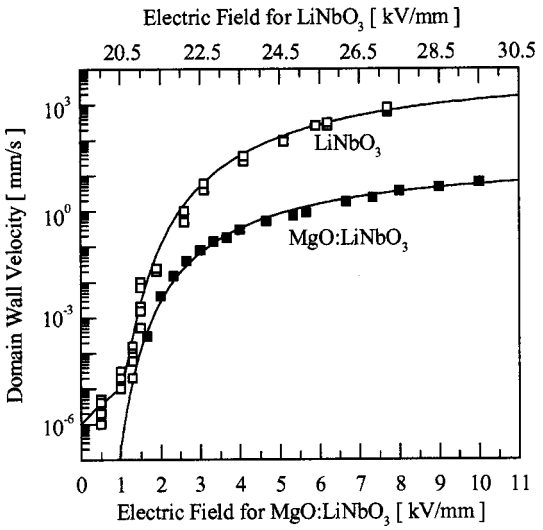

FIG. 1. Domain wall velocity as a function of electric field. The squares are the experimental results for MgLN and LN. The solid lines are the fitting curves. Note that the curves have different abscissae.

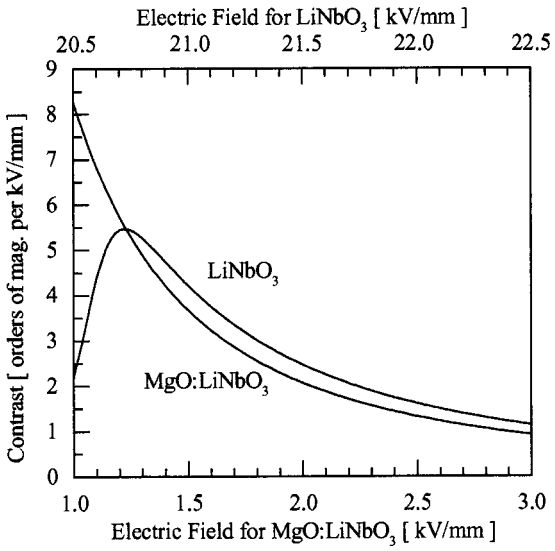

FIG. 2. Derivative of the log of the solid lines in Fig. 1 gives the contrast curves shown. The contrast is the sensitivity of the domain wall velocity to change in the electric field.

By applying the poling field, independently nucleated domains merged and formed a flat wall with a length of around 5 mm. The following domain wall velocity measurement was done on this merged wall. Gopalan *et al.* reported that the domain wall velocity of the merged wall is faster than that of the independent domain by one or two orders.[18] Since in periodic poling, domains tend to nucleate along electrode edges, where there is a fringing field, and form a flat wall, our method of measurement is expected to be suitable for predicting the behavior during periodic poling. Figure 1 shows the domain wall velocity as a function of the poling field. The poling field was varied from 1.7 to 10 kV/mm; the domain wall velocity changed by four orders of magnitude over this range. The duration of the poling field was varied from 1 ms to 10 s to obtain measurable progress of domain walls. The relationship between the domain wall velocity v (mm/s) and the electric field E (kV/mm) was fit well by the following relation

$$v(E) = 38.0 \exp(-19.0/E). \tag{1}$$

The fitting function has a similar form to that reported in $BaTiO_3$.[15] In Fig. 1, the velocity–field curve for LN (Ref. 17) is also shown for comparison. Note that Fig. 1 has different abscissae for the two materials. The velocity–field curve for LN has an offset of about 20.5 kV/mm, and has a tail for fields lower than this value. As is discussed next, the higher electric-field range (>20.5 kV/mm) where the curve is steep is important for periodic poling. The fitting function in this region is given by

$$v(E) = 16\,300 \exp(-25.0/(E-19.2)). \tag{2}$$

It is obvious from the Fig. 1 that MgLN can be poled at lower electric fields than those used for LN. For well-defined periodic poling, it is necessary to terminate the domain inversion at an electric field at which domain wall velocity is sensitive to changes in the electric field, i.e., a negative feedback mechanism exists. A contrast curve (derivative of the log of the field–velocity curve) gives a quantitative estimation of the sensitivity of the domain wall velocity to the electric field. The contrast curves of MgLN and LN are shown in Fig. 2. Note that Fig. 2 again has different abscissae for the two materials. MgLN has the same order of contrast as LN, but at a significantly lower range of electric fields. The contrast of MgLN is of order five at $E = 1.3$ kV/mm while LN requires 20.7 kV/mm to attain the same value. This reduced field is beneficial for periodic poling because the problem of dielectric breakdown during poling can be avoided.

III. DESIGN OF PERIODIC POLING CONDITIONS

In electric-field poling, the main objective is to obtain a specified domain period and duty cycle with acceptable uniformity throughout the volume of the crystal. While the domain period is assured by the lithography which produces the electrode patterns, domain duty cycle is determined by control of the domain wall propagation during the domain inversion. To optimize the domain duty cycle, the relationship between the domain wall velocity and the applied electric field given by Eq. (1) is used to determine the optimum conditions of periodic poling, namely the electrode geometry and poling voltage wave form. A computational model was employed to simulate the domain wall propagation under different poling conditions.[17] For convenience, we reproduce here the key elements of the analysis in Ref. 17. The kernel of the model is an equation yielding the domain duty cycle as a function of time, referred to as the equation of domain wall motion:

$$DC(t) = \frac{2}{\Lambda} \int_0^t \nu(E_0[DC(\tau);\mathbf{u}])\, d\tau + DC(0), \tag{3}$$

where $DC(t)$ is domain duty cycle as a function of time t, $DC(0)$ is an initial duty cycle, (i.e., a ratio of the electrode width to the domain period), $v(E)$ is domain wall velocity as a function of average field given by Eq. (1), $E_0[DC(t);\mathbf{u}]$ is

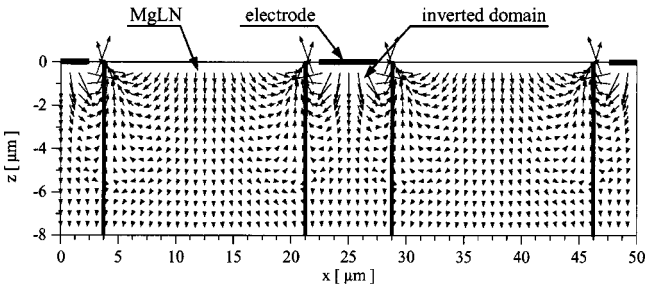

FIG. 3. Vector field plot showing the fringe fields for MgLN with 7.5-μm-wide domains spread 1.25 μm beyond each electrode edge. The fourth root of the field magnitude is plotted to provide visibility for low field regions. The parameters for the calculation are summarized in Table I.

the average field in the ferroelectric as a function of domain duty cycle, **u** is a vector of geometric and dielectric parameters, and Λ is the domain period. The definition of the vector **u** is given in the appendix.

In electric-field poling, domain nucleation occurs at the edges of the electrodes, after which the inverted domains progress both inward and outward from the edge of the electrode. The main purpose of the computational model is to describe the behavior of the domain wall propagation outward from the electrode edge to under the insulator. The domain duty cycle $DC(t)$ in this calculation is defined as the ratio between the distance of the outward domain wall from the electrode center and half the grating period. Thus, the initial duty cycle $DC(0)$ is taken as the electrode duty cycle. The electric field $E_0(DC;\mathbf{u})$ averaged over a domain wall is calculated with an electrostatic model whose key result is the decrease in the average electric field resulting from unscreened polarization charge that appears under the insulator after domain reversal. Figure 3 shows an example of a vector electric-field plot in MgLN. The calculation conditions are summarized in Table I. In the calculation, it was assumed that the crystal surface is covered by an insulator and the voltage is applied through periodic electrodes. It was also assumed that MgLN has the same dielectric constants as those for LN ($\varepsilon_{xf}=85.2$ and $\varepsilon_{zf}=27.8$). Figure 3 shows a vector field plot when 7.5-μm-wide inverted domains spread 1.25 μm beyond each edge of the 5-μm-wide electrode. As is seen from Fig. 3, as domains spread out from under the electrodes, the unscreened spontaneous polarization charge deposited on the surface of the crystal reverses the sign of

TABLE I. Calculation parameters for the vector field plot shown in Fig. 3.

Parameter	Measurement
Grating period Λ	25 μm
Electrode width w_e	5 μm
Crystal thickness t_f	300 μm
Insulator thickness t_i	2 μm
Relative permittivity of ferroelectric for x polarized field ε_{fz}	85.2
Relative permittivity of ferroelectric for z polarized field ε_{fz}	28.7
Relative permittivity of insulator ε_i	3.0
Spontaneous polarization P_s	0.78 μC/mm^2
Electrode voltage v_e	2 kV

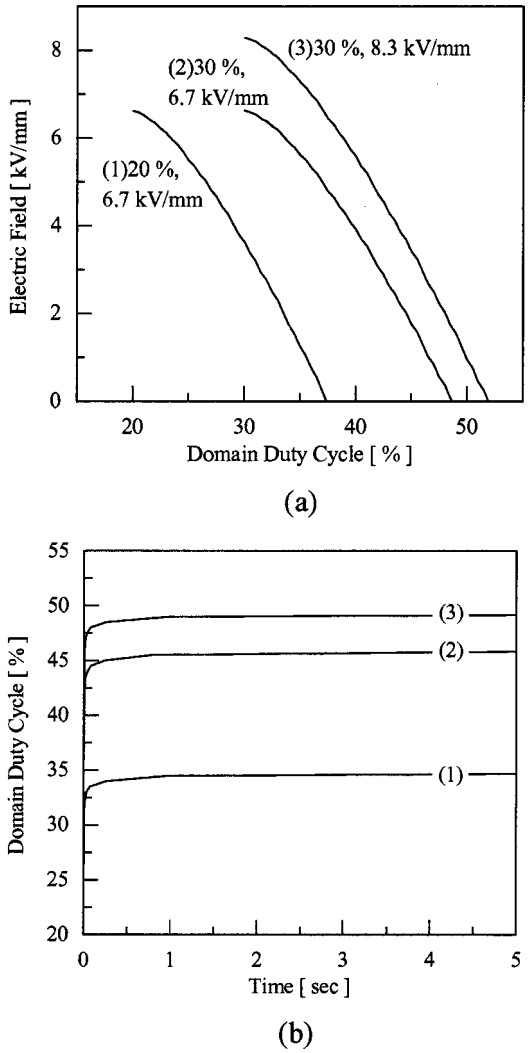

FIG. 4. (a) Average electric field at the domain wall as a function of domain duty cycle. The curves were calculated for different initial conditions of the electrode duty cycle and the electric field. (b) Temporal variation of the domain duty cycle. The curves were calculated by using the data shown in Fig. 4(a) in Eqs. (1) and (3).

the z component of the electric field in the vicinity of the crystal surface, and more importantly, reduces the average field encountered by the domain wall through the thickness of the wafer. The reduction in the average electric field slows the growth of the domain, due to the strong dependence of the velocity on the electric-field amplitude. Figure 4(a) shows the change of the average electric field at the domain wall as a function of the domain duty cycle for periodic poling with a period of 25 μm. The curves in Fig. 4(a) correspond to different initial values of electrode duty cycle and voltage applied to the electrodes. As the inverted domain grows, the average electric field at the domain wall decreases due to the unscreened spontaneous polarization charge. By putting the data given in Fig. 4(a) into Eq. (3), the domain duty cycle $DC(t)$ as a function of time is derived and is shown in Fig. 4(b). Since the domain wall velocity changes by orders of magnitude with small changes in the electric field, the growth of the domain wall is self-terminated at a certain duty cycle which is determined by the initial condition. In this example, 50% domain duty cycle is achieved

with the electrode duty cycle of 30% and the electric field of 8.3 kV/mm. The advantage of self-termination is that since the domain growth is controlled locally by choosing an optimum electrode geometry and poling voltage wave form, it is possible to minimize the influence of defects and to maximize the uniformity of the duty cycle. This model accurately predicts the dynamics of poling in congruent lithium niobate, as shown in detail in Ref. 17. As is discussed in Sec. IV, the model also works well for MgLN, with one qualification. In CLN, the initial nucleation of domains occurs on a time scale short compared to the rest of the poling process, so it is not necessary to account for it in the dynamical model; as would be expected under these conditions, the poling current decreases monotonically with time after the spike of displacement current at the beginning of the process. As discussed in Sec. IV, for MgLN, the current grows slowly in the initial stages of poling, presumably reflecting a domain nucleation process that is occurring on a time scale comparable to that of the entire poling process. Once this nucleation stage is completed, the predictions of the model are again in reasonable accord with observations, so that it remains useful for designing a self-terminating process.

IV. PERIODIC POLING OF MgLN

Periodic poling of MgLN was done by the conventional electric-field method. A periodic electrode pattern was fabricated on the $+z$ surface of wafer with photoresist (Shipley, S1818). The thickness of the photoresist was 2 μm and the grating period was 25 μm. After lithography, the wafer was postbaked at 120 °C for 10 h to remove the solvent from the photoresist to enhance its dielectric strength. The wafer was then loaded into an electrolyte-containing fixture. The electrolyte used was a saturated solution of LiCl in deionized water. On the $+z$ surface, the electrolyte contacted the MgLN only at the openings in the photoresist. The electrolyte uniformly contacted on the $-z$ surface. The voltage wave form was programmed by an arbitrary wave from generator (Stanford Research Systems, DS345). The output of the wave form generator was amplified by a high voltage amplifier (Trek, Model 20/20), and the high voltage was applied to the MgLN through the electrolyte. The current through the wafer was monitored by a 10 kΩ resistor connected in series to ground.

Figure 5 shows typical traces of the poling voltage and current. The conditions used to produce these curves are: crystal thickness = 0.3 mm, electrode period = 25 μm, electrode width = 4.5 μm, and poling voltage = 2 kV (6.7 kV/mm). With these parameters, a final duty cycle calculated by the model mentioned above was 35%. Although 50% duty cycle is ideal for the QPM devices, the design duty cycle was set to 35% to avoid unwanted merging of domains. The poled area was an 11-mm-diameter circle (95 mm^2). No significant poling current was observed at 1 kV (3.3 kV/mm). When the poling voltage was increased to 2 kV, a poling current was observed, which increased gradually from zero after the displacement current (sharp spike in the trace at $t = 1$ s), reached its peak 1.15 s after the spike. The peak current was 110 μA. The decrease of the poling current after the main peak indicates the self-termination of domain wall propagation. In the periodic poling experiments, we also observed that the domain nucleation rate depends on the applied electric field. For example, when the electric field was decreased from 6.7 to 5 kV/mm, the poling current decreased by an order of magnitude, requiring ten times the poling time for the same area, while the domain wall velocity is decreased by only a factor of two (see Fig. 1). After periodic poling, the sample was etched in hydrofluoric acid for 5 min to reveal the domain inversion by selective etching of the $-z$ surface. Figure 6 shows the microscope image of the etched sample. The view shows the former $+z$ surface; the inverted and uninvested domains in one cycle are indicated in the Fig. 6. The grating vector was set to be parallel to the crystal x axis to align the domain walls with the straight edges of the natural hexagonal domain shape. The periodic domain inversion was fairly uniform over the poled area, and there was no merging of the domains on either the $+z$ or the $-z$ surfaces. Most of the inverted domains were self-terminated at a duty cycle of about 50%, somewhat larger than the 35% predicted by the model. As is seen from the Fig. 6, some domain walls

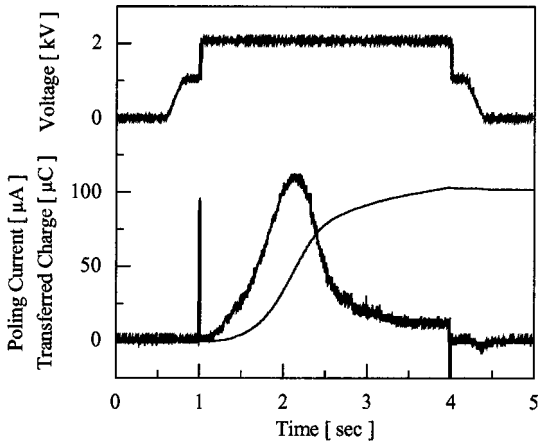

FIG. 5. Poling voltage and current traces in the periodic poling of MgLN. The transferred charge is the integral of the poling current.

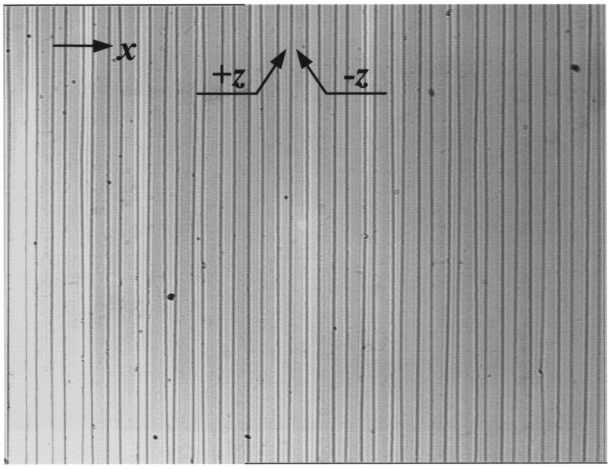

FIG. 6. Etched surface (originally $+z$) of the PPMgLN. The grating period is 25 μm. There was no merging of the domains on either the $+z$ or $-z$ surfaces over the 11-mm-diameter poled area.

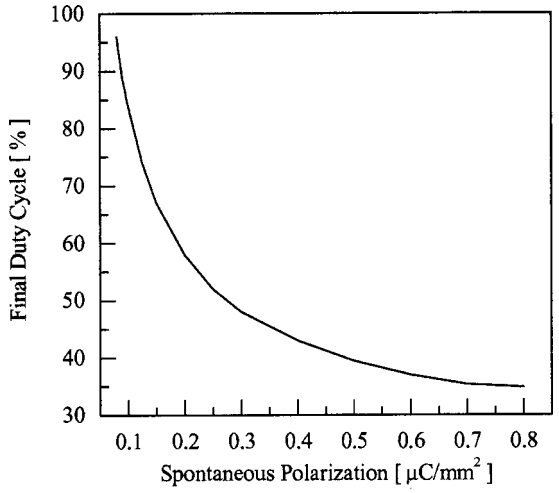

FIG. 7. Calculated final duty cycle of periodically poled domains as a function of the effective spontaneous polarization for poling conditions as were used in the experiment.

were not straight, resulting in local duty cycles of about 70%. Possible reasons for the overpoling are discussed in the Sec. V.

V. DISCUSSION

Here we discuss the overpoling from two points of view: leakage current and postbake conditions. As is mentioned herein, the sample was periodically poled with 50% duty cycle while the computational model predicted 35% duty cycle. We again note that the model produces quantitatively correct results for LN while the behavior of MgLN is more complex. In this case, it appears that the overpoling may be attributed to the leakage current that exists in addition to the poling current. As reported in Ref. 17, the leakage current in LN is negligible compared to the poling current, while for MgLN, as is seen in Fig. 5, the total current has a significant tail after the poling process is completed. Even when a longer voltage pulse (30 s) was applied, this current did not decrease to zero. It also shows a nonohmic characteristic which is seen from the decrease of the current from 12 μA to almost zero at $t=4$ s when the poling voltage was decreased from 2 to 1 kV. Sonoda *et al.* reported the diode-like current–voltage characteristics of MgLN after periodic poling[10] which is similar to the phenomenon in our experiment. If the leakage current exists, it is expected that the unscreened surface charge which is essential for the self-termination is reduced. As a first-order approximation, the reduction of the unscreened surface charge can be included in the computational model by reducing the value of the spontaneous polarization. Figure 7 shows the final duty cycle as a function of the spontaneous polarization. The calculation parameters are identical to the experimental conditions mentioned in Table I except for the spontaneous polarization. The calculation predicts that the final duty cycle is increased as the spontaneous polarization becomes smaller. In the experiment, the final duty cycle was 50% which corresponds to an equivalent spontaneous polarization of 0.28 μ C/mm^2, which is 36% of the measured value of 0.78 μ C/mm^2. With the poled area of 95 mm^2, it is estimated that the surface charge was reduced by 48 μC because of the leakage current. This reduction of surface charge is consistent with the leakage current level of 12 μA for 4 s of poling time. We again note that the model produces quantitatively correct results for LN without the need for such correction factors, indicating that MgLN has. To investigate the influence of the leakage current on the poling result in detail, it is necessary to characterize the dependence of the current on the local fields, and develop a corresponding dynamic model for the domain wall motion, which we have not yet completed.

Another factor complicating the poling of MgLN is the complex dependence on the thermal history prior to poling. As is seen in Fig. 6, a few domain walls are not straight, resulting in some regions where the local duty cycle is about 70%. A reason for this overpoling is microscopic inverted domains (microdomains) formed during the postbake of the photoresist for the patterned electrode. During the cooling stage in the postbake, surface charge is pyroelectrically induced on the crystal surface. The electric field associated with the charge is large enough to cause nucleation of microdomains, whose diameter is typically less than 10 μm. To examine the influence of the postbake on the poling quality, we tested two conditions: postbake with and without an electrically conductive plate above the sample. We use such a conductive plate in our standard process for poling LN to prevent the formation of pyroelectrically induced microdomains during the baking of the photoresist, by neutralizing the surface charge with the glow discharge that develops in the high field region between the sample surface and the conductive plate, here a glass plate coated with chromium. Figure 8(a) shows a crossed Nicol image of a sample postbaked *without* the conductive plate. The bright spots are microdomains formed during the postbake. Their density was about 300 sites/mm^2. The dark strips are the photoresist mask for the segmented grating patterns, with a grating period of 15 μm and segment widths of 130μm for the upper six gratings in Fig. 8(a) and the segment widths of 30 μm for the lower seven gratings. The sample was then poled and etched in hydrofluoric acid. A microscope image of the etched surface is shown in Fig. 8(b), showing uniform poling over the entire area. Figure 9(a) shows a crossed Nicol image of the sample postbaked *with* the conductive plate. It is clear that the use of the conductive plate suppressed the formation of the microdomains, as their density was reduced by a factor of ten. The sample was poled and etched as before, with the etched surface shown in Fig. 9(b). Although, as intended, the number of microinverted domains after the postbake was suppressed by use of the conductive plate, the poling resulted in a nonuniform pattern of periodically poled domains. This result is in marked contrast to that obtained in LN, where the suppression of the microdomains with the glow discharge does reduce small-scale inhomogeneity associated with the microdomains and does not lead to such patchy areas of periodic poling. The nonuniform pattern was also observed when a longer voltage pulse (duration$=30$ s) was applied. The difference in the poling results made by the postbake conditions was also observed with a uniform grating pattern and with a longer grating period of 25 μm. The origin of this

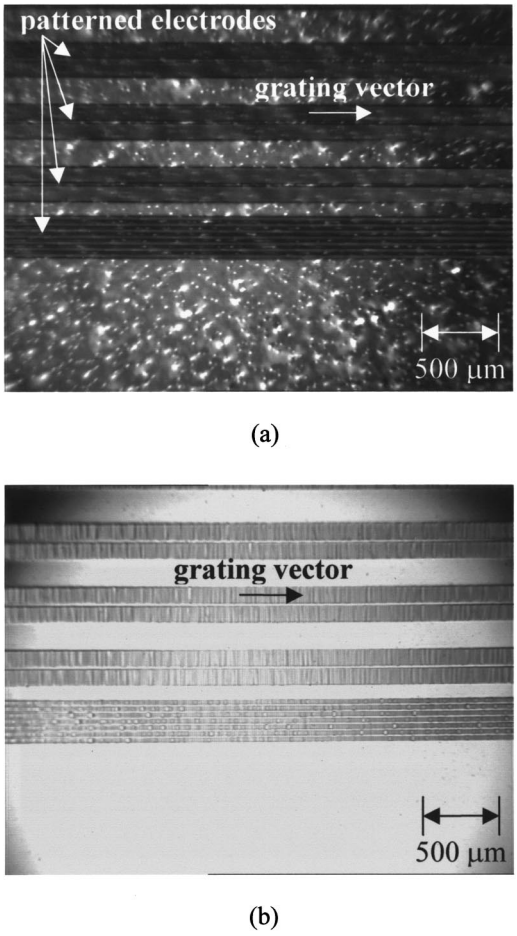

FIG. 8. (a) Crossed Nicol image of a sample postbaked *without* a conductive plate. The bright spots are the microdomains caused by the pyroelectric effect during the cooling stage in the postbake. (b) After the sample shown in Fig. 8(a) was poled, the sample was etched. This figure shows the etched surface of the sample.

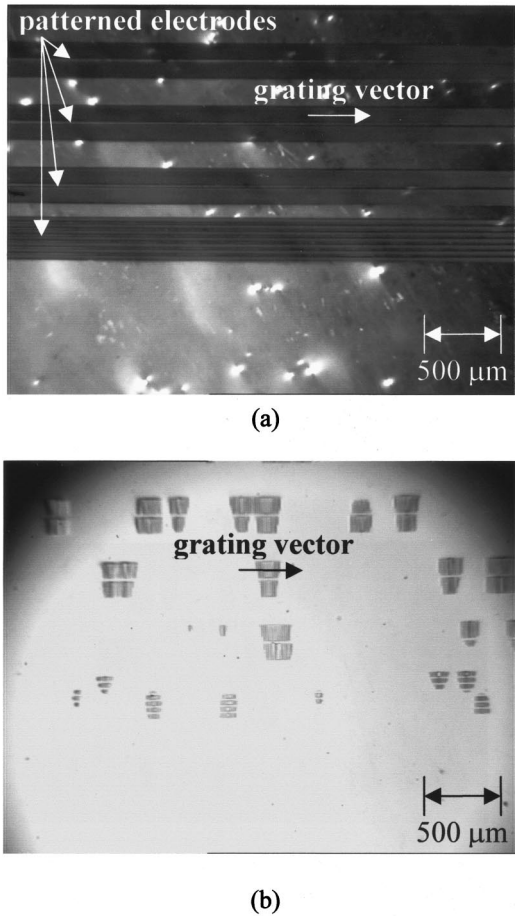

FIG. 9. (a) Crossed Nicol image of a sample postbaked *with* a conductive plate. The use of the conductive plate suppressed the number of microdomains by an order of magnitude as compared to the sample shown in Fig. 8(a). (b) The etched surface of the poled sample. Periodic poling resulted in nonuniform pattern of periodically poled regions.

distinction between the behavior of LN and MgLN is not yet clear.

VI. CONCLUSION

We investigated the poling characteristics of MgLN and demonstrated fabrication of well-defined PPMgLN by the self-terminating method. In the experiment, PPMgLN with grating periods ranging from 15 to 25 μm were fabricated with good uniformity. It was found that thermal history prior to poling of MgLN has a significant influence on the poling quality. The physical origin of this phenomenon is not clear. Spectroscopic and electrostatic studies of the sample before and after annealing would help explain the observation. Development of an optimum postbake condition with which uniform periodic poling is obtained and the formation of microdomains is minimized is currently under investigation.

Since MgLN can be poled at low electric field, periodic poling of thicker samples is of interest for high power operation of QPM optical frequency converters. The periodic poling condition for a thick sample (thickness$>$1 mm) can be also determined by the model described here. PPMgLN is also attractive for short wavelength (blue/green) generation by second-harmonic generation since it has a higher photorefractive damage threshold and less green-induced infrared absorption than does LN. These applications require short (2–5 μm) grating periods. Conditions of self-termination for these periods can be also examined by the model. For example, the fabrication of a 5-μm-period, 0.5-mm-thick PPMgLN requires an electrode width of 1 μm and poling field of 5 kV/mm to achieve 50% final duty ratio in the model. Another application of PPMgLN is waveguide QPM devices. While there have been several reports of blue light generation by waveguide PPMgLN, its use in optical frequency mixers for telecommunications applications such as all-optical wavelength conversion, spectral inversion, and time-gated mixing[19–21] has yet to be explored.

ACKNOWLEDGMENTS

The authors would like to acknowledge Dr. Gregory D. Miller who developed the computational model described in this article in the course of the research reported in his dissertation, Ref. 17. This work was undertaken at Ginzton Laboratory, Stanford University while one of the authors (K.N.) was a visiting scholar on leave from Research Insitute of Electrical Communication, Tokyo University, funded by the Ministry of Education, Culture, Sports, Science, and Technology of Japan.

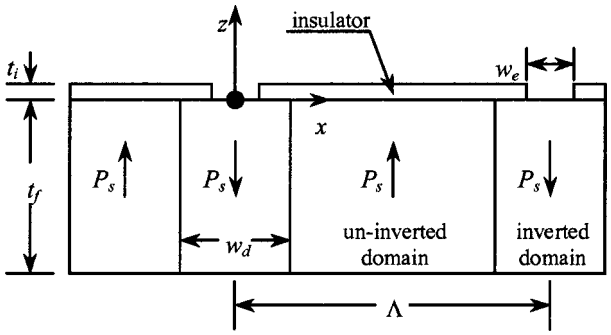

FIG. 10. Poling configuration and variables used to calculate fields and potentials.

This research was sponsored by the Air Force Office of Scientific Research, Air Force Material Command, USAF, under AFOSR Grant No. F49620-99-1-0270.

APPENDIX

In this appendix, a definition of the vector **u** in Eq. (3) of the domain wall motion is discussed. Figure 10 shows the cross section view for a ferroelectric with a periodic array of electrodes lithographically defined on its $+z$ face with an insulator. Here, we assume that the poling field is applied with an electrolyte through periodic openings in the insulator. During periodic poling, as domains spread out from under the electrodes, the unscreened spontaneous polarization charge deposited on the surface of the crystal reverses the sign of the z component of the electric field in the vicinity of the crystal surface. Thus, the potential along the interface is specified only on the electrodes, while charge is specified along the interface between the electrodes. These potentials and the surface charge density are used as boundary conditions to calculate the electric-field distribution in the ferroelectric. The vector **u** is a set of conditions which are necessary to calculate the field distribution in the ferroelectric in addition to the boundary conditions. The vector **u** consists of the following parameters: The electrolyte is held at a uniform potential ν_e. The z axis is parallel to the z axis of the original single-domain ferroelectric. The minus z face of the ferroelectric ($z=-t_f$) is held at the reference potential, 0 V, also typically using an electrolyte contact. In Fig. 10, the direction of the spontaneous polarization P_s is shown for both the uninverted and inverted domains of the ferroelectric. The thickness of the insulator is t_i. The domain duty cycle is defined $DC=w_d/\Lambda$, and the electrode duty cycle is defined $DC_e=w_e/\Lambda$. The material parameters which define the vector **u** are: relative permittivity of insulator ϵ_{xi} and relative permittivity of the ferroelectric; ϵ_{xf} and ϵ_{zf} for the x and z polarized field, respectively. A variety of numerical techniques can be used to calculate the field distribution. To generate the vector field plot as shown in Fig. 3 in this article, we chose to use a computational method based on a finite Fourier transform taking advantage of the periodicity of the electric field, whose details are discussed in Ref. 17. Table I shows a set of parameters to generate the vector field plot.

[1] D. A. Bryan, Robert Gerson, and H. E. Tomaschke, Appl. Phys. Lett. **44**, 847 (1984).
[2] Y. Furukawa, K. Kitamura, S. Takekawa, K. Niwa, and H. Hatano, Opt. Lett. **23**, 1892 (1998).
[3] A. Harada and Y. Nihei, Appl. Phys. Lett. **69**, 2629 (1996).
[4] A. Harada, Y. Nihei, Y. Okazaki, and H. Hyuga, Opt. Lett. **22**, 805 (1997).
[5] K. Mizuuchi, K. Yamamoto, and M. Kato, Electron. Lett. **32**, 2091 (1996).
[6] K. Mizuuchi, K. Yamamoto, and M. Kato, Electron. Lett. **33**, 806 (1997).
[7] K. Mizuuchi, H. Ohta, K. Yamamoto, and M. Kato, Opt. Lett. **22**, 1217 (1997).
[8] K. Mizuuchi and K. Yamamoto, Opt. Lett. **23**, 1880 (1998).
[9] T. Sugita, K. Mizuuchi, Y. Kitaoka, and K. Yamamoto, Opt. Lett. **24**, 1590 (1999).
[10] S. Sonoda, I. Tsuruma, and M. Hatori, Appl. Phys. Lett. **23**, 3078 (1997).
[11] S. Sonoda, I. Tsuruma, and M. Hatori, Appl. Phys. Lett. **21**, 3048 (1997).
[12] A. Kuroda and S. Kurimura, Appl. Phys. Lett. **69**, 1565 (1997).
[13] Y. Hirano, S. Yamamoto, and H. Taniguchi, Technical Digest of Conference on Lasers and Electro-Optics 2001 (Optical Society of America, San Francisco, 2001), pp. 579–580.
[14] M. Nakamura, M. Sugihara, M. Katoh, H. Taniguchi, and K. Tadamoto, Jpn. J. Appl. Phys., Part 2 **38**, L1234 (1999).
[15] R. C. Miller and A. Savage, Phys. Rev. **115**, 1176 (1959).
[16] R. G. Batchko, V. Y. Shur, M. M. Fejer, and R. L. Byer, Appl. Phys. Lett. **75**, 1673 (1999).
[17] G. D. Miller, Ph.D. dissertation, Stanford University, 1998.
[18] V. Gopalan, S. S. A. Gerstl, A. Itagi, T. E. Mitchell, Q. X. Jia, T. E. Schlesinger, and D. D. Stancil, J. Appl. Phys. **86**, 1638 (1999).
[19] M. H. Chou, I. Brener, M. M. Fejer, E. E. Chaban, and S. B. Christman, IEEE Photonics Technol. Lett. **11**, 653 (1999).
[20] M. H. Chou, I. Brener, G. Lenz, R. Scotti, E. E. Chaban, J. Shmulovich, D. Philen, S. Kosinski, K. R. Parameswaran, and M. M. Fejer, IEEE Photonics Technol. Lett. **12**, 82 (2000).
[21] K. R. Parameswaran, M. Fujimura, M. H. Chou, and M. M. Fejer, IEEE Photonics Technol. Lett. **12**, 654 (2000).